

EXTREME-ULTRAVIOLET FLARE LOOP EMISSIONS IN AN ERUPTIVE EVENT

JIONG QIU, HAIMIN WANG, JONGCHUL CHAE and PHILIP R. GOODE
Big Bear Solar Observatory, New Jersey Institute of Technology, Big Bear City, CA 92314, U.S.A.

(Received 26 November 1999; accepted 28 January 2000)

Abstract. The TRACE/BBSO joint campaign on 27 September 1998 observed an eruptive flare event which lasted for half an hour. The observation covered several ultraviolet (UV) and extreme-ultraviolet (EUV) lines and $H\alpha$ center and off-band emissions with very high spatial resolution. We find the EUV emissions in different stages of the flare display different characteristics. (1) During the 'pre-flare' phase, when the SXR output was weak, we observed simultaneous impulsive HXR peak at 25–100 keV and strong EUV emission. (2) In the impulsive phase, when $H\alpha$, UV and SXR emissions were rising to the maxima, the EUV emission was very weak. (3) During the main phase, when SXR emission was decaying, a peak in the EUV emission was observed which was substantially delayed by 7 min compared to emissions from other wavelengths. Based on our observations, we propose that the 'pre-flare' phase in this event was a separate energy release process rather than a mere pre-cursor of the flare, and it is likely that the 'pre-flare' EUV emission was due to weak *in situ* heating of low-lying coronal loops. The mechanism of the EUV emission in the main phase is investigated. It is suggested that the delayed EUV emission may come from cooling of SXR loops.

1. Introduction

The solar transition region connecting the cool chromosphere and hot corona has been investigated through observations of UV and EUV emissions. In the study of solar flares, the relation of UV and EUV emissions to emissions at other wavelengths has been an important issue.

For lower-temperature plasmas, early observations frequently demonstrated the close temporal and spatial correlation between broadband EUV (10–1030 Å) emissions, impulsive UV emissions, and hard X-ray bursts in solar flares (Donnelly, 1969; Donnelly and Kane, 1978; Widing, 1982; Cheng and Pallavicini, 1987; Poland *et al.*, 1982, 1984). A modified version of the thick-target model, namely, the partial precipitation model, was hence proposed in which the hard X-ray correlated broadband emission is due to the electron-beam bombardment in the cool region embedded in the chromosphere (McClymont and Canfield, 1986; LaRosa and Emslie, 1988; Laming and Feldman, 1992). But Cheng (1990) also found the impulsive UV component prior to the hard X-ray burst and proposed electric current heating in the loop before the acceleration of hard X-ray electrons.

At higher temperature (but still lower than SXR temperature), both impulsive and gradual components of EUV emissions have been reported (Horan and Kreplin, 1981; Horan, Kreplin, and Dere, 1983; Neupert, 1989). Observations by Cheng



and Widing (1975) suggested that the hot ($>10^6$ K) SXR flare loop gradually cooled down to emit at temperatures of a few times 10^5 K. For one type of solar flares, i.e., two-ribbon flares, extensive investigations have been made on the thermal evolution of flare loops (Schmieder *et al.*, 1995, and references therein). Based on observations, the flare model developed by Carmichael (1964), Sturrock (1966), Kopp and Pneuman (1976) and its later modifications (Forbes, Malherbe, and Priest, 1989; Forbes and Acton, 1996) are greatly favored. This model suggests that the flare plasmas emitting at soft X-ray temperature at the beginning of the flare are cooled down during the thermal evolution to emit at EUV and UV lines and eventually at $H\alpha$ temperatures.

But for this cooling scenario, observational evidence linking the SXR stage to the EUV stage is generally missing. Arguments by Feldman and Seely (1995) recently questioned this scenario. Some other observations also seem to suggest that cool and hot loops in some solar flare events were not identical, while the physical link between them was unclear (Cheng, 1980). Although studies of flare loop evolution have mostly been concentrated on two-ribbon flares, one would expect the same physics to hold in other types of flares.

From various observations, questions have been raised which have not been settled: what are the origins of the transition region UV and EUV emissions? Are they from the primary energy release process or the secondary effect of energy transfer? Are the plasmas seen emitting in UV and/or EUV lines the same plasmas emitting soft X-ray and/or $H\alpha$? If yes, is the variation in different wavelengths simply a temporal evolution of the same plasma under the same physical process? If no, what is the physical relation between higher and lower temperature plasmas, and what is the physical environment for these plasmas?

In this paper, an eruptive flare observed by Big Bear Solar Observatory (BBSO) and the Transition Region And Corona Explorer (TRACE) will be presented. TRACE, launched in 1998, is to-date the most powerful UV and EUV imager. It affords the best spatial resolution ever with reasonable time cadence which reveals a vivid picture of the dynamic solar transition region in very fine scales (Handy *et al.*, 1999). We discuss the different stages of energy release in this flare which gave rise to different thermal and dynamic features of the flare plasma most distinctively seen in UV and EUV emissions.

2. Observations

During the joint observation campaign between TRACE and BBSO on 27 September 1998, the active region NOAA 8340 (N21 W52) was selected as the target from 16:00 UT to 19:00 UT. It was a decaying complex region dominated by a single spot of positive leading polarity which was surrounded by faint negative plages. Several small satellite spots of negative polarity were visible to the east of the major spot. Figure 1 shows a line-of-sight magnetogram of the active region.

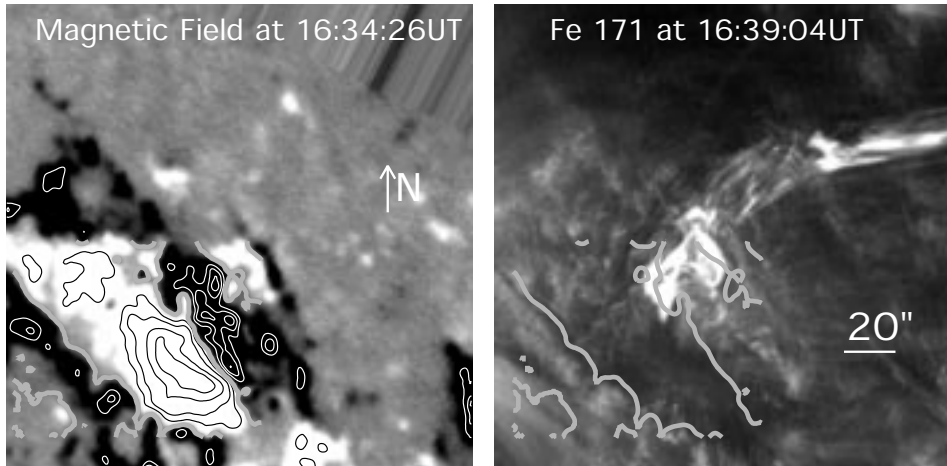


Figure 1. *Left*: longitudinal magnetic field; dark line indicates the positive field intensity (contour level: 200, 400, 800, 1200 G) and white line indicates the negative field (contour levels: -400 , -300 , -200 G); thick grey line is the longitudinal inversion line. *Right*: eruptive flare observed at TRACE Fe IX 171 Å line at 16:39:04 UT on 27 September 1998; the thick grey line indicates the inversion line of the longitudinal field.

TABLE I
TRACE temperature response (Handy *et al.*, 1999)

Wavelength (Å)	Emission	Bandwidth (Å)	Temperature (K)
171	Fe IX/X	6.4	$1.6-2.0 \times 10^5$
195	Fe XII/XXIV	6.5	$5.0-20 \times 10^5$
1550	C IV	30	$6.0-25 \times 10^4$
1600	UV Cont, C I, Fe II	275	$4.0-10 \times 10^3$
1700	Continuum	200	$4.0-10 \times 10^3$
5000	White light	broad	$4.0-6.4 \times 10^3$

In this region, many micro-flares were detected by TRACE (Wang *et al.*, 1999). At 16:20 UT, an eruptive C5.2/1F flare occurred, as shown in Figure 1.

TRACE observed this event with its high cadence mode in emission lines at C IV 1550 Å, Fe IX 171 Å, Fe XV 195 Å and broad-band continua at 1600 Å and 1700 Å, and white light. The wavelengths, bandwidths, and formation temperatures of the above emission lines are shown in Table I. The data thus obtained cover the temperature range from 10 000 K to 2 MK. The time cadence is about 100 s for one complete run over all spectral lines, and the pixel resolution is $0.5''$ within a FOV of $256'' \times 256''$ for the C IV line and continuum and $512'' \times 512''$ for hot Fe lines. The white-light images are used to co-align TRACE and BBSO observations.

Simultaneous BBSO observations include: the high-resolution filtergrams at $H\alpha$ line center and $H\alpha \pm 0.65 \text{ \AA}$ with a time cadence of 1.5 min for each wavelength and with a FOV of $256'' \times 256''$, the videomagnetograms (VMG) with a cadence of a few minutes and with a FOV of about $320'' \times 245''$, and full disk $H\alpha$ line center images with a cadence of 1 min and a pixel resolution of $1''$.

The slight shift between TRACE EUV and white light images is corrected by using the offset values from a preliminary analysis of TRACE data (Handy *et al.*, 1999). In order to remove the image shift in the time sequence due to the rotation of the Sun, a cross-correlation algorithm is applied. Then the TRACE and BBSO images are co-aligned by registering the common features of the sunspot group present in both TRACE and BBSO images. The accuracy of the alignment is subject to the seeing condition and the best precision that can be achieved with images of good resolution is about $1''$.

3. Time Evolution

3.1. NEUPERT EFFECT

Figure 2 gives the light curves of the flare emissions at all observed wavelengths. The GOES SXR light curve actually showed three emission peaks, two minor C1 class peaks at 16:27 UT and 16:33 UT followed by the major C5.2 peak at 16:42 UT, implying the existence of several stages of energy release in this event. To check the ‘Neupert effect’ (Neupert, 1968; Dennis and Zarro, 1993), the time derivative of GOES 1–8 \AA emission is plotted in Figure 2(a), showing three peaks which we dub as ‘Neupert peaks’ in the following text. For this flare, a BATSE HXR observation was obtained, but only till 16:27 UT when the satellite night started. The HXR impulsive burst peaking at 16:26:40 UT was correlated with the first ‘Neupert peak’ (Figure 2(a)). Assuming that the lower chromosphere, during the flare, is heated by non-thermal electron beams which produce impulsive enhancement in $H\alpha$ red wing (Fisher, Canfield, and McClymont, 1985), we may use the $H\alpha$ red-wing light curve (Figure 2(c)) in place of HXR emission to check for the Neupert effect. Figure 2 shows a clear temporal correlation between SXR time derivative and $H\alpha$ offband emission at the moments of the first and third ‘Neupert peaks’. The correlation for the second peak was not as clear because of the slowly-varying nature of the emissions at this time.

An additional check comes from the fact that in the images of white-light continuum, sudden brightening was observed at the moments of the first and third ‘Neupert peaks’, which indicates heating of the deep chromosphere by penetrating non-thermal electrons. The temporal correlation between the ‘Neupert peaks’, $H\alpha$ red wing emission, and impulsive brightening in the deep chromosphere suggests that acceleration of non-thermal electrons was involved in both the pre-flare phase and the impulsive phase.

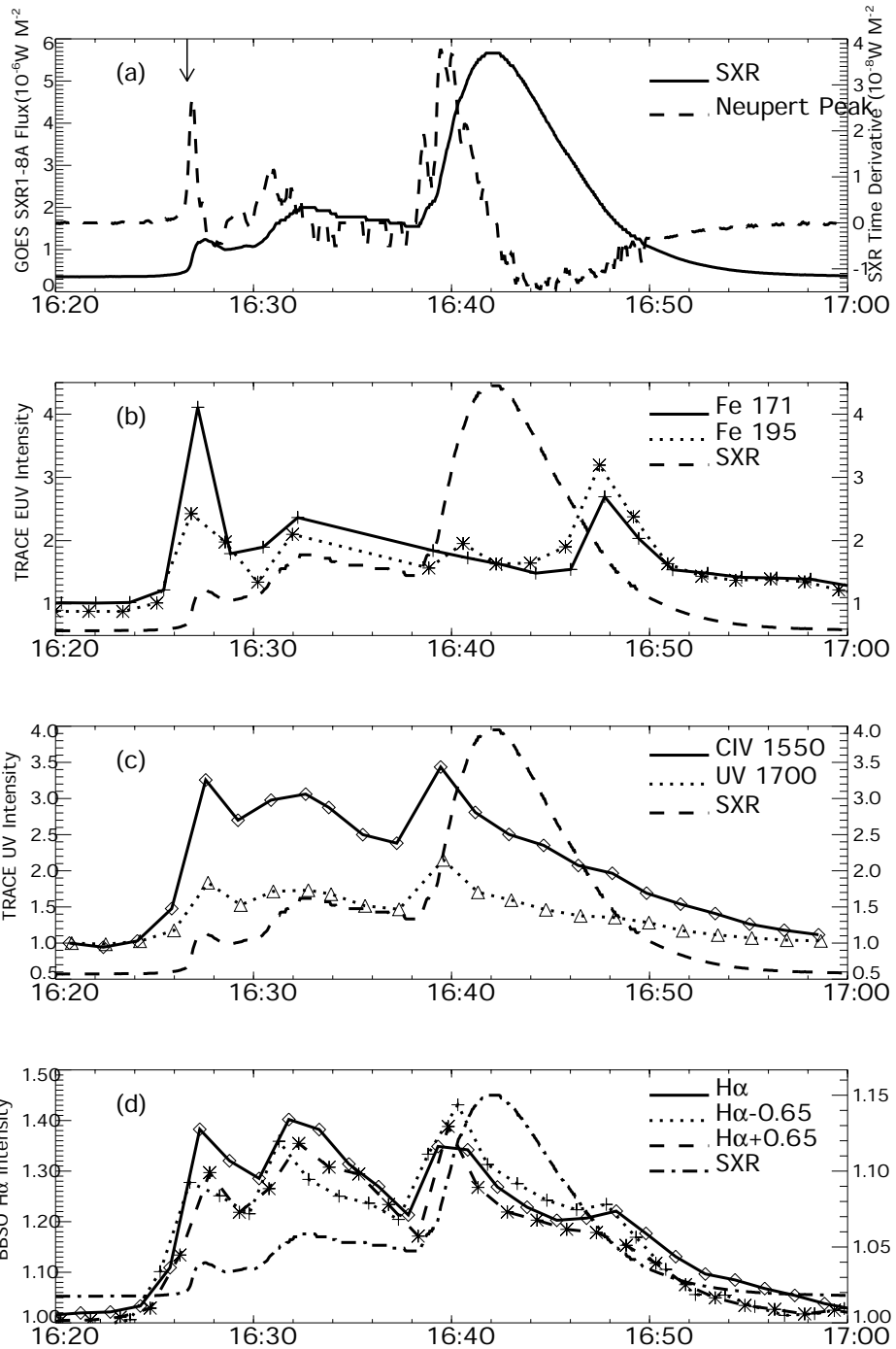


Figure 2. From top to bottom: time profiles of the flare at SXR, EUV, UV, and H α wavelengths. EUV/UV/H α emissions are normalized to pre-flare and quiet-region intensity. The arrow in the first panel indicates the time of BATSE HXR peak. The SXR light curve in the second to fourth panels is in arbitrary units.

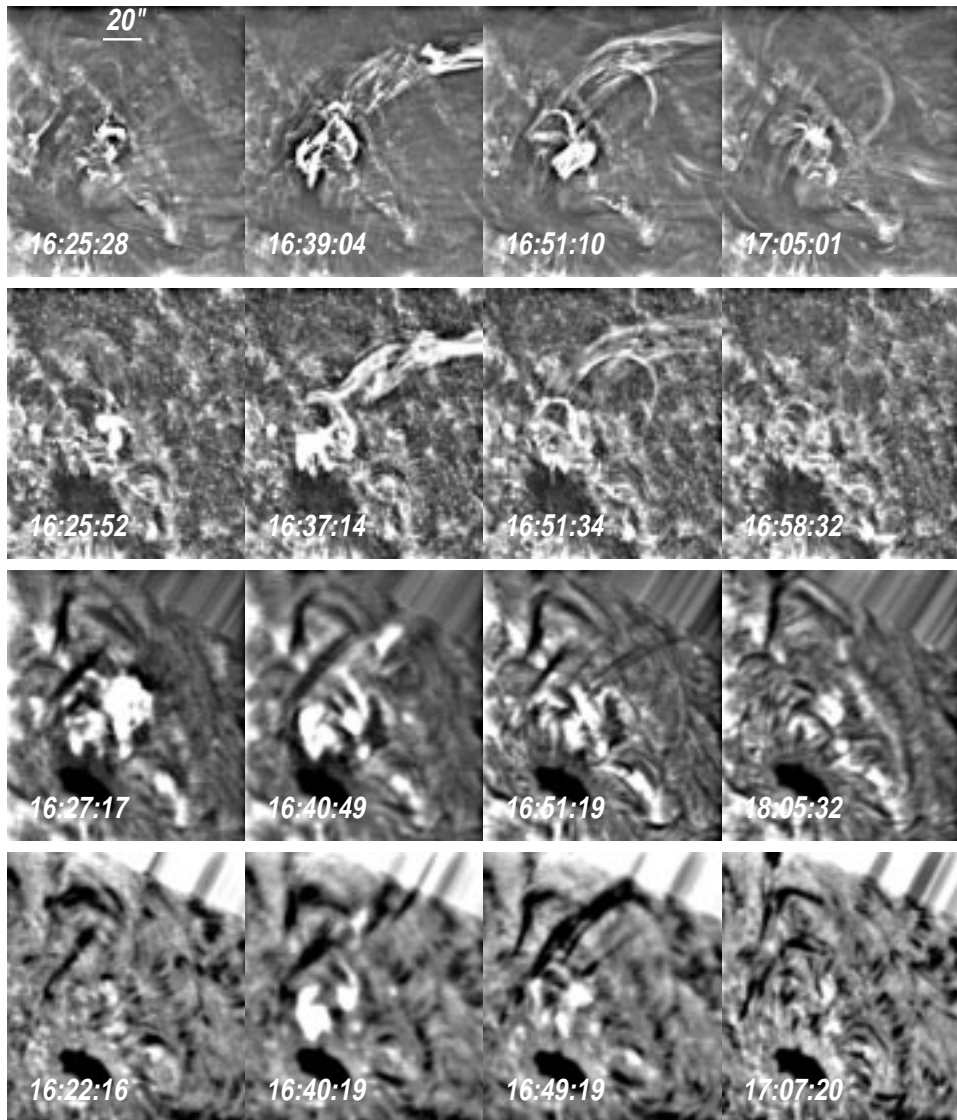


Figure 3. From top to bottom: evolution of the flare at Fe IX 171 Å, C IV 1550 Å, H α , H α - 0.65 Å.

3.2. EUV EMISSION

The story was different for emissions in EUV lines. Seen from Figure 2(b), roughly three peaks can be also identified. The rise and fall of the first EUV spike were simultaneous with the first Neupert peak within the time resolution of the observing facilities, while the third EUV peak was delayed by 7 min compared with the third Neupert peak. Such a difference indicates that in the two stages of energy release mentioned above, the mechanisms involved may be different which gave varying

multi-spectral temporal behaviors. Due to the data gap from 16:32–16:39 UT in EUV channels, it is hard to identify the time of the second EUV peak.

It is noteworthy that although the intensities of $H\alpha$, UV, and EUV emissions at the first stage were comparable with the third stage emission, GOES SXR observation showed a much weaker emission peak in the first stage. In studies of solar flares, the stage of weak heating prior to the main impulsive phase is often observed as the pre-flare phase; however, in this event, observations imply that the ‘pre-flare’ phase was not a simple pre-cursor of the following major energy release, but a separate energy release process in a different manner from the major phase.

3.3. MASS EJECTION AND SPREAD OF FLARE

Between the two impulsive ‘Neupert peaks’, at the chromosphere and transition region, flaring spread from the initial site to extended regions giving rise to enhanced emissions at all wavelengths, especially in the $H\alpha$ line. The light curves at all wavelengths showed slow rise and fall which seems to exclude the scenario of non-thermal electron acceleration in this stage.

4. Locations of UV and EUV Emissions

Figure 3 demonstrates the morphologic evolution of the event. The time sequence of the flare showed the following features: (1) collisions and disruptions of low-lying coronal loops seen in EUV which started the flare and mass ejection; (2) mass ejections visible in all wavelengths immediately after the flare started; (3) flaring in extended areas in the active region as seen in all wavelengths; (4) appearance of new EUV loops towards the end of the flare. As found in Section 3, different stages of energy release were involved in this event and distinct differences were shown in the temporal behavior of the EUV emissions. In this section, the details of the different stages are studied separately.

4.1. PRE-FLARE PHASE

4.1.1. *UV and $H\alpha$*

A minor C1 SXR peak was recorded prior to the main phase of the flare. At the time of the 25–100 keV HXR burst, two compact kernels were clearly seen in $H\alpha$ center and offband images and TRACE UV images at C IV 1550 Å and 1600/1700 Å continuum. Further, TRACE white-light images show brightening at 16:27:46 UT at one of the chromospheric kernels. These signatures demonstrate the well-known scenario that the deep chromosphere at the foot points of the magnetic loop, was promptly heated by non-thermal electron beams which are also responsible for the hard X-ray emission through thick-target bremsstrahlung (Brown, 1971).

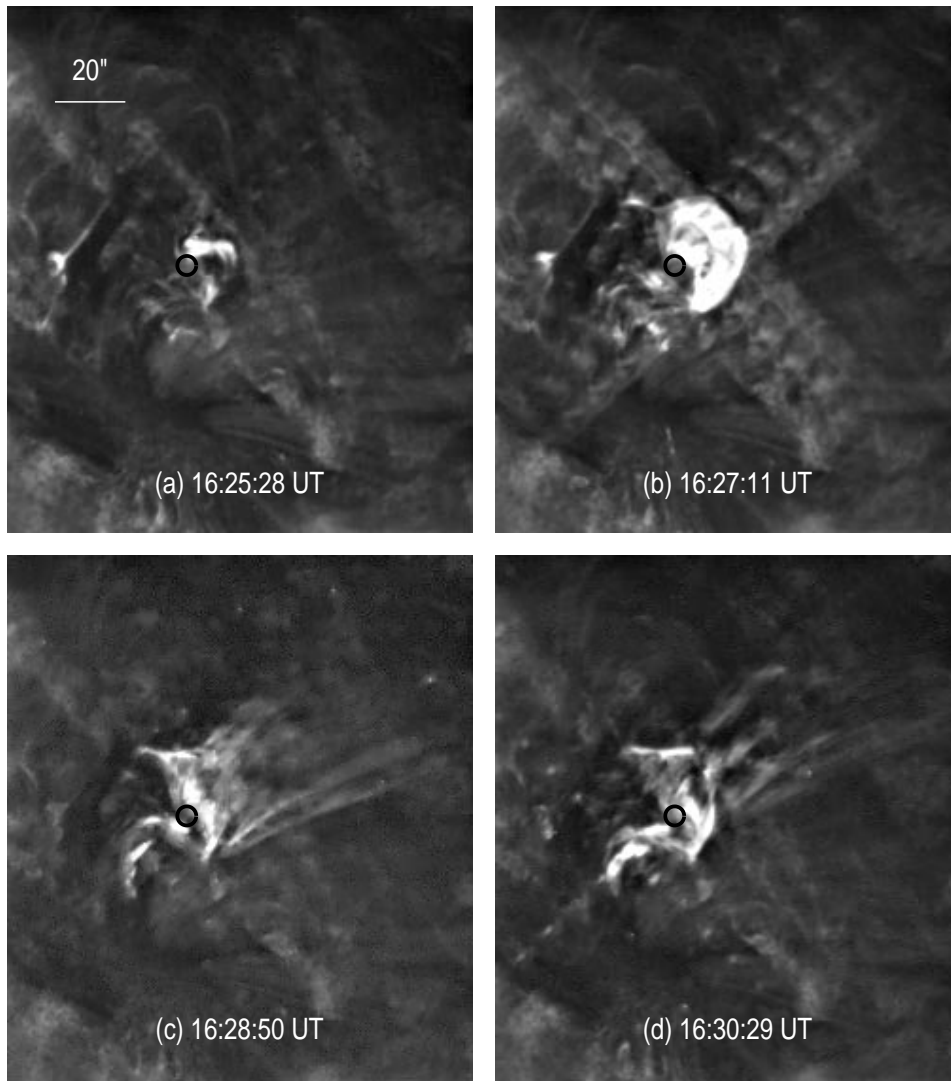


Figure 4. Evolution of the flare at Fe IX 171 Å in the 'pre-flare' phase showing interacting EUV loops and disruption of the field. The circle indicates the position of brightening in white-light continuum at 16:27:46 UT.

4.1.2. EUV

At the time of the hard X-ray emission, the brightest feature in the EUV images was two or more low-lying, slightly inclined and interacting EUV loops (Figure 4(a)) which resulted in the expansion (Figure 4(b)) and explosion (Figure 4(c)) of the loops. The lower-temperature emission sources were well co-aligned at the foot regions of these EUV loops (Figure 4). The lack of delay in the EUV emission

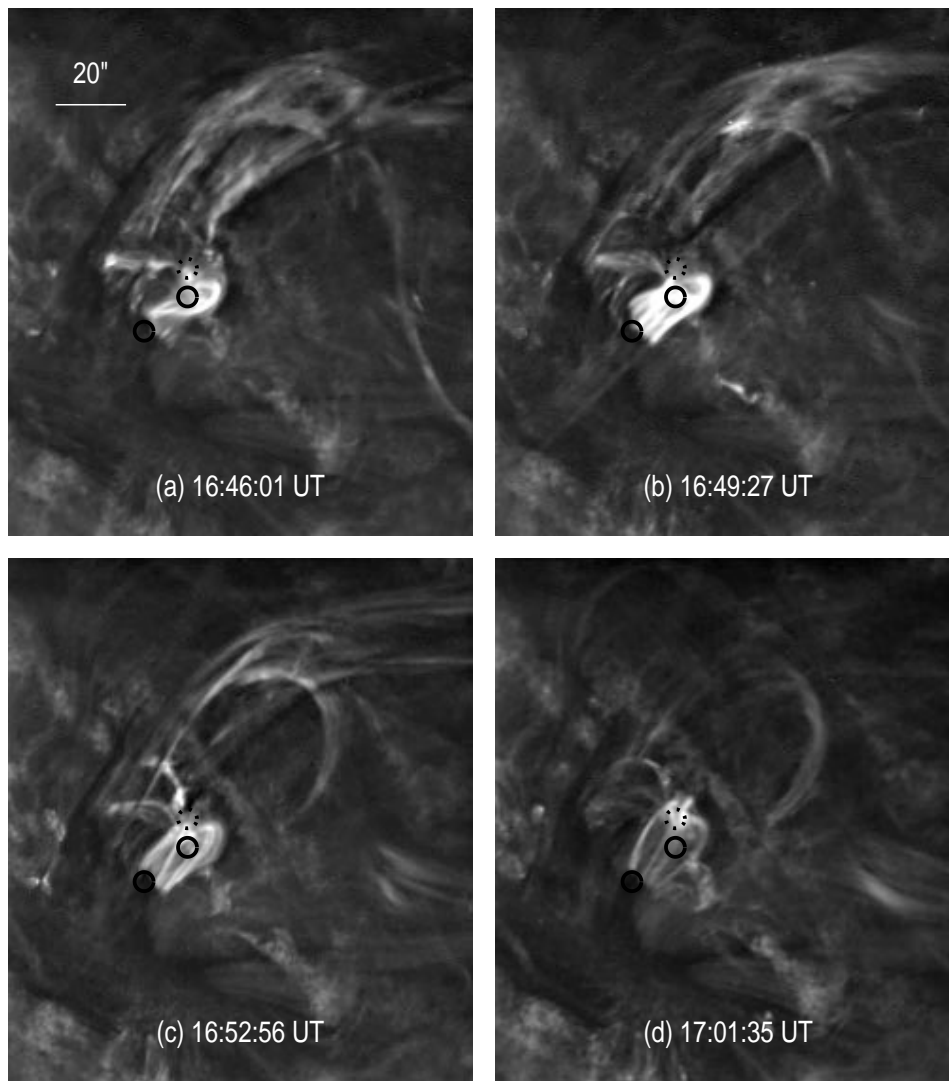


Figure 5. Evolution of the flare at Fe IX 171 Å after the major SXR emission showing the formation and cooling of EUV loops. The solid circles indicate brightening in white-light continuum at 16:39:39 UT and the dotted circle indicates the position of the continuum brightening in the pre-flare phase (see Figure 4).

with respect to the HXR burst indicates the *in situ* heating of these interacting low-lying loops, which were probably subsequently disrupted and erupted.

4.2. MAIN PHASE

4.2.1. *UV and H α*

Prior to the SXR maximum, the impulsive ‘Neupert peak’ was simultaneous with the emission maximum at H α off-band, C IV line and UV continuum. TRACE white-light images, for the second time, displayed brightening at 16:39:39 UT in two kernels co-aligned with the site of H α and UV kernels which confirms the strong heating of the deep chromosphere.

4.2.2. *EUV*

After the SXR maximum, a sudden appearance of a set of EUV loops was observed at Fe XII 195 Å and Fe IX 171 Å. Figure 5 demonstrates the brightening of the EUV loops. These loops faded in half an hour’s time. Again, we found the brightening of the kernels observed in UV continuum, H α and white-light emission located exactly at the feet of these EUV loops which implies a physical relation between the two. However, different from the first stage, the appearance of EUV loops was delayed by 7 min after the second ‘Neupert peak’ and the footpoint region impulsive brightening.

4.3. MASS EJECTION

The flare was also spectacular in its eruptive features in all wavelengths. This is different from the often observed flare-associated surges which are usually cool. The ejected materials in this event were clearly seen at UV and EUV wavelengths as emitting plasmas.

Figure 6 illustrates the emission from the ejected materials. The time profiles suggest continuous heating along the loops from 16:30–16:42 UT. Careful examination of the UV and EUV images reveals that the emissions at UV and EUV came from the same plasmas heated along the large-scale loops. This fact restricted the temperature range of the ejected plasmas to 10^5 – 10^6 K which cannot be observed by GOES.

5. Mechanisms of UV and EUV Emissions

5.1. UV EMISSIONS

Throughout the event, emissions in UV continuum at 1600/1700 Å and H α wings (especially the red wing), either impulsive or gradual, showed similar time profiles. In certain stages, the impulsive enhancement in the lower atmosphere was also correlated with HXR bursts and ‘Neupert peaks’ prior to the SXR emissions. This agrees with the previous broadband UV and EUV observations in past decades (Donnelly, 1969; Donnelly and Kane, 1978). During the event, the emission sources of the UV continuum, like in H α off-band, were located at the foot regions of the

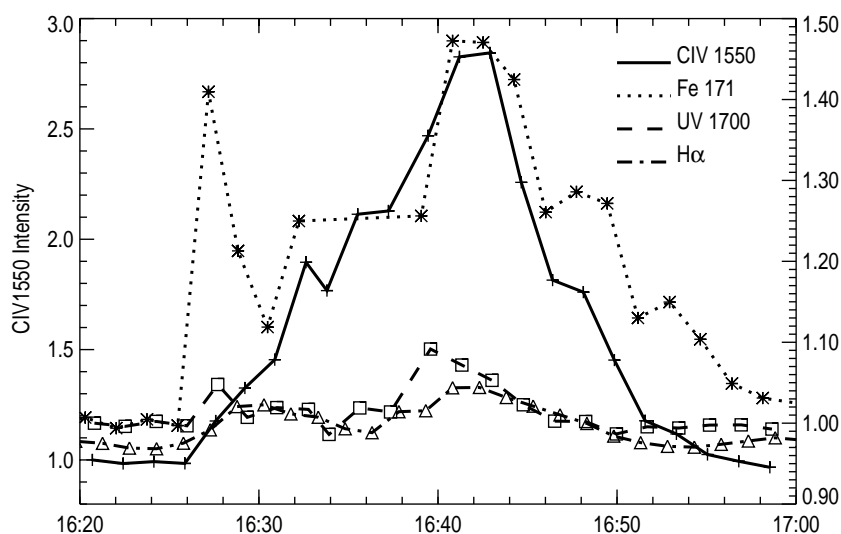


Figure 6. Time profiles of the eruption at EUV/UV/H α wavelengths. The intensities are all normalized to pre-flare and quiet regions.

EUV loops. It thus confirms that the precipitation model is valid for UV continuum emissions (McClymont and Canfield, 1986; LaRosa and Emslie, 1988; Laming and Feldman, 1992). The C IV 1550 Å emission at footpoint regions exhibited all these characteristics as well, which indicates the same heating mechanism in the flaring chromosphere and lower transition region.

The C IV 1550 Å emission in this flare also came from an optically thin source along the large-scale magnetic loops. There are several possibilities concerning the heating mechanism: heating by shock waves generated during the mass ejection, heating by slow reconnection between mutually inclined over-lying coronal field lines, or heating by reconnection between over-lying coronal field and the field lines brought from below by the eruption.

5.2. EUV EMISSIONS

For optically thin Fe lines, we can decide whether or not EUV emissions in these lines came from the coronal magnetic loops which had no counterparts in lower temperature emissions. We propose a weak *in situ* heating scenario for the EUV emission in the first stage of the eruption. The EUV emission peak is strong compared to the SXR emission, which indicates that in this stage, heating was not sufficient to produce an appreciable amount of plasma emitting in SXR.

During the main phase, the apparent delay between SXR and EUV emissions suggests that the EUV emission could be due to cooling of the SXR emitting plasma. Indirect evidence for this comes from the fact that the impulsive emissions in UV, H α and white-light continuum prior to SXR emission were located at the

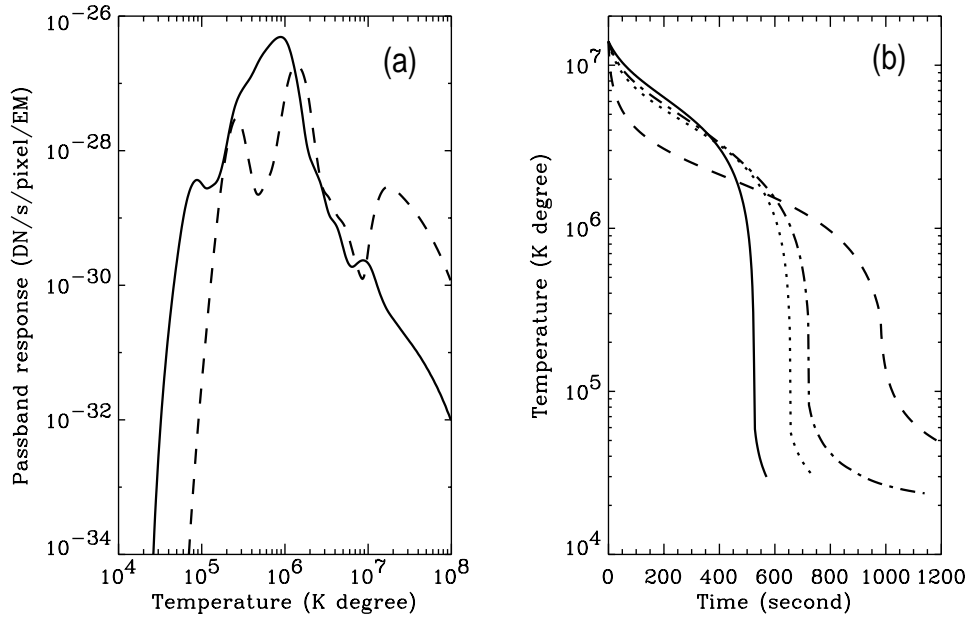


Figure 7. (a) The TRACE Fe IX 171 Å (solid line) and Fe XII 195 Å (dashed line) response as a function of temperature (at the electron density of 10^{10} cm $^{-3}$). (b) Temperature evolution of coronal loop plasmas at constant densities of 1×10^{11} (solid line), 5×10^{10} (dotted line), 1×10^{10} cm $^{-3}$ (dot-dashed line) and time varying density (dashed line) obtained from GOES. The initial temperature is 14 MK and the scaling height is 16 000 km.

two feet of the EUV loops which were formed later. Suppose that the major emission peak in SXR was produced by the same process of energy release which also is responsible for the non-thermal heating at the chromosphere, it follows that SXR loops must be formed at the same location of the EUV loops, with the footpoint regions heated by non-thermal beams.

Figure 7(a) illustrates the temperature response at Fe IX 171 Å and Fe XII 195 Å obtained from the CHIANTI data base (Dere *et al.*, 1997). Plasmas of a wide temperature range from 10^5 K to 10^7 K will contribute to the emissions at Fe IX 171 Å and Fe XII 195 Å (Handy *et al.*, 1999), but the emission maximum at about 1×10^6 K cannot be detected by GOES. Since at the time of EUV emission peak there was no observational sign of enhanced SXR emission, the EUV emission should come from plasmas of temperature lower than a few times 10^6 K for which GOES is not sensitive.

Supposing that SXR loops were formed during the main phase, we may estimate the cooling time of the hot SXR loops. Two cooling mechanisms are considered, namely conductive cooling and radiative cooling. In the absence of a continuous heating, the temperature evolution of the SXR loops is governed by the equation

$$\frac{dT}{dt} = -\frac{\epsilon(T)n_e^2}{3kn_e} - \frac{1.1 \times 10^{-6}T^{7/2}}{3kn_eL^2}, \quad (1)$$

where $\epsilon(T)$ is the temperature dependent radiative cooling function, n_e is the electron density, L is the temperature scaling height and k is Boltzmann constant. From GOES two-channel diagnostics, the initial temperature at 16:40 UT is taken as 14 MK. For plasmas at a temperature $3 \times 10^5 < T < 3 \times 10^7$ K, we use an empirical formula for $\epsilon(T)$ (Raymond *et al.*, 1976),

$$\epsilon(T) = 1.2 \times 10^{-19} T^{-1/2} . \quad (2)$$

For temperatures lower than 3×10^5 K, the cooling function is taken as (McClymont and Canfield, 1983)

$$\epsilon(T) = 3.8 \times 10^{-37} T^3 . \quad (3)$$

Figure 7(b) illustrates the temperature evolution of the hot SXR loop for different densities. It is shown that from 14 MK to a few times 10^6 K, conductive cooling dominates so that the cooling time scales for different densities do not differ significantly. It takes less than 8 min to cool the hot plasma to 3×10^6 K, and about 10 min to cool to 2×10^6 K, which may explain the observed time delay of EUV emissions. The plasma at a temperature lower than 3×10^6 K is already beyond GOES's sensitivity.

At the lower temperature, the cooling of the loops is controlled by radiative losses, hence the cooling time scales vary at different densities. If we assume the plasma emits from a constant volume, the decaying curve of EM derived from GOES gives the decaying electron density. In this case, below 2×10^6 K, the cooling time is much longer than in the case of constant loop density. The observed lifetime of EUV loops was longer than 20 min which agrees better with the case of the time varying density.

The cooling scenario mentioned above encounters a difficulty in explaining the decreasing density of the loop plasma. Further, the decreasing SXR EM derived from GOES may not be solely due to a decreasing density, but the volume of the emitting plasma may change as well. If a constant loop density is maintained, an additional heating source would be needed to explain the observed lifetime of EUV loops.

6. Summary

In this paper, observations of an eruptive flare on UV, EUV and $H\alpha$ were studied. We find different stages of energy release in this flare producing different kinds of EUV emissions. The results are summarized in the following:

(1) In the 'pre-flare' phase, we find impulsive hard X-ray, UV, EUV emissions and deep chromosphere heating, suggesting that the 'pre-flare' phase in this event was not a simple precursor of the major flare but indicated a separate energy release process. The EUV emissions in this phase appeared to be caused by a weak *in situ* heating of low-lying coronal loops.

(2) The major flare occurred at a slightly different location from the ‘pre-flare’ phase. In the impulsive phase, characterized by the rise of SXR emission and enhanced H α and UV emissions, we only observed a very weak EUV emission.

(3) During the main phase, sudden brightening of new EUV loops was observed, which gave rise to the enhanced EUV emission. The EUV emission in this phase was delayed by 7 min with respect to the impulsive phase emissions at UV and H α lines and by 5 min compared to the SXR maximum. Our analysis suggests that the brightening of these EUV loops was due to cooling of SXR plasmas.

Acknowledgements

We are grateful to the BBSO staff and TRACE team who successfully performed the joint observing campaign. The author J.Q. thanks J. Lin for helpful discussions. The work is supported by NSF under grants ATM-9628862 and ATM-9713359, and by NASA under grants NAG5-5036 and NAG5-7085, and ONR under grant N00014-97-1-1037.

References

- Brown, J. C.: 1971, *Solar Phys.* **18**, 489.
- Carmichael, H.: 1964, in W. N. Hess (ed.), *AAS-NASA Symposium on the Physics of Solar Flares*, NASA-SP **50**, p. 451.
- Cheng, C. C.: 1980, *Astrophys. J.* **238**, 743.
- Cheng, C. C.: 1990, *Astrophys. J.* **349**, 362.
- Cheng, C. C. and Pallavicini, R.: 1987, *Astrophys. J.* **318**, 459.
- Cheng, C. C. and Widing, K. G.: 1975, *Astrophys. J.* **201**, 735.
- Dennis, B. R. and Zarro, D. M.: 1993, *Solar Phys.* **146**, 177.
- Dere, K. P., Landi, E., Mason, H. E., Monsignori Fossi, B. C., and Young, P. R.: 1997, *Astron. Astrophys. Suppl.* **125**, 149.
- Donnelly, R. F.: 1969, *Astrophys. J.* **158**, L165.
- Donnelly, R. F. and Kane, S. R.: 1978, *Astrophys. J.* **222**, 1043.
- Feldman, U. and Seely, J. F.: 1995, *Astrophys. J.* **450**, 902.
- Fisher, G. H., Canfield, R. C., and McClymont, A. N.: 1985, *Astrophys. J.* **289**, 425.
- Forbes, T. G. and Acton, L. W.: 1996, *Astrophys. J.* **459**, 330.
- Forbes, T. G., Malherbe J. M., and Priest, E. R.: 1989, *Solar Phys.* **120**, 285.
- Handy, B. N., Acton, L. W., Kankelborg, C. C. *et al.*: 1999, *Solar Phys.* **187**, 229.
- Horan, D. M. and Kreplin, R. W.: 1981, *Solar Phys.* **74**, 265.
- Horan, D. M., Kreplin, R. W., and Dere, P.: 1983, *Solar Phys.* **85**, 303.
- Kopp, R. A. and Pneuman, G. W.: 1976, *Solar Phys.* **50**, 85.
- Laming, J. M. and Feldman, U.: 1992, *Astrophys. J.* **386**, 364.
- LaRosa, T. N. and Emslie, A. G.: 1988, *Astrophys. J.* **326**, 997.
- McClymont, A. N. and Canfield, R. C.: 1986, *Astrophys. J.* **305**, 936.
- Neupert, W. N.: 1968, *Astrophys. J.* **153**, L59.
- Neupert, W. M.: 1989, *Astrophys. J.* **344**, 504.
- Poland, A. I., Frost, K. J., Woodgate, B. E., Shine, R. A., Kenny, P. J., Machado, M. E., Cheng, C. C., and Tandberg-Hanssen, E. A.: 1982, *Solar Phys.* **78**, 201.

- Poland, A. I., Orwig, L. E., Mariska, J. T., Auer, L. H., and Nakatsuka, R.: 1984, *Astrophys. J.* **280**, 457.
- Raymond, J. C., Cox, D. P., and Smith, B. W.: 1976, *Astrophys. J.* **204**, 290.
- Schmieder, B., Heinzel, P., Wiik, J. E., Lemen, J., Anwar, B., Kotrč, P., and Hiei, E.: 1995, *Solar Phys.* **156**, 337.
- Sturrock, P. A.: 1966, *Nature* **211**, 695.
- Wang, H., Chae, J., Qiu, J., Lee, C., and Goode, P. R.: 1999, *Solar Phys.* **188**, 367.
- Widing, K. G.: 1982, *Astrophys. J.* **258**, 835.